Article:
Han, L., Mao, J., Cao, P. et al. (2022) Toward Sensorless Interaction Force Estimation for Industrial Robots Using High-Order Finite-Time Observers. IEEE Transactions on Industrial Electronics, 69 (7). pp. 7275-7284. ISSN: 0278-0046

https://doi.org/10.1109/tie.2021.3095820

Towards Sensorless Interaction Force Estimation for Industrial Robots Using High-Order Finite-Time Observers

Linyan Han, Jianliang Mao, *Member, IEEE*, Pengfei Cao, Yahui Gan, and Shihua Li, *Fellow, IEEE*

***Abstract*—This paper proposes a novel interaction force estimation scheme capable of estimating the interaction forces for industrial robots with high precision in the absence of force sensors. Specifically, we first establish the dynamic model of a class of industrial robots via model identification methods. Furthermore, a high-order finite-time observer (HOFTO) is established to estimate the interaction forces, where HOFTO serves as an interaction force observer and is designed to accurately estimate external time-varying interaction forces. In addition, we strictly analyze the stability of our approach in two different cases, endowing HOFTO with reliable estimation abilities in broader applications. Subsequently, we integrate the estimated force information into the applications of force control frameworks (e.g., collision detection and impedance control). Several evaluations on a real 6-axes robot demonstrate the effectiveness of the proposed approach.**

***Index Terms*—Interaction force estimation, high-order finite-time observer, parameter identification, force control.**

I. Introduction

In a myriad of applications, such as deburring [1] and guiding tasks [2] as well as collision detection [3], robot manipulators need to contact with external environments properly and thus careful treatment of interaction forces is vital. In force-sensitive scenarios, traditional approaches on position control are prone to impose strong stiffness using large control gains and consequently the risk of breaking robots and harming environments becomes high. In order to overcome this issue of position-control methods, force control has been studied towards obtaining an environment or user-friendly controller, where interaction forces between robots and the environment are taken into account. Usually, interaction forces are measured by a force/torque sensor. However, the high price of force sensors restricts their applicability in various settings. Moreover, the deployment of force sensors per se also increases the difficulty of structural design. Therefore, an efficient and easily-implemented interaction force observer has great potentials, which indeed has been showcased in many previous works [4], [5], [6].

A straightforward way of estimating interaction forces is to utilize the motor torque, position, velocity and acceleration information [7]. However, this kind of approaches will become problematic since double differentiation of position signals amplifies measurement noise in practice. Therefore, various filters [8] were employed to improve the estimation accuracy of interaction forces, which, however, brings another issue, i.e., the small time delay caused by the filter will prolong the system's response time.

In order to address the aforementioned issues, many alternative solutions have been investigated [9], [10], [11], [12]. In [9], a nonlinear disturbance observer was proposed to estimate the interaction forces. The stability and performance of the reaction torque observer in a robust force control system were analyzed, where the estimation of environmental impedance control through the reaction torque observer can be viewed as an application of disturbance observers [10], [11]. In [12], an extended state observer (ESO) was applied to estimate the interaction forces with a theoretical analysis. However, these works only focus on estimating constant or slow time-varying interaction forces while the case of fast time-varying interaction forces (e.g., in highly dynamical environments) has not been explored sufficiently.

Based on the design idea of finite time convergence, the super-twisting algorithm (STA) observer [13] is designed to estimate the interaction forces and has achieved great success. However, the STA observer is first-order and can only accurately estimate the interaction forces with the first-order derivative bounded. However, the interaction forces in practice are complex and changeable, so it is desired to design an interaction force observer with the ability of generalization.

In this paper, we are dedicated to the design of a force observer so as to estimate time-varying (particularly fast time-varying) interaction forces, with the aim of addressing the limitations of the aforementioned approaches. Specifically, using an identified dynamics model of robot manipulators, we design a HOFTO to estimate the interaction forces in a finite time horizon. The proposed interaction force observer not only guarantees the global stability, but also provides a

This work was supported in part by the National Natural Science Foundation (NNSF) of China under Grants 61973081, 62025302, and 61873308 and The Fundamental Research Funds for the Central Universities under Grant No. 202008003, and the Key R & D plan of Jiangsu Province under Grant BE2020082-4.

Linyan Han, Pengfei Cao, Yahui Gan and Shihua Li (corresponding author) are with the School of Automation, Southeast University, Key Laboratory of Measurement and Control of Complex Systems of Engineering, Ministry of Education, Nanjing 210096, PR China (corresponding author: +86 025-83793785; e-mail: lsh@seu.edu.cn).

Jianliang Mao is with the College of Automation Engineering, Shanghai University of Electric Power, Shanghai 200090, PR China, and also with the R & D Institute of ESTUN AUTOMATION CO., LTD, Nanjing 211106, PR China.

more accurate estimation in comparison with the traditional ESO-based methods. The main contributions of this paper include

1) *An observer design method is utilized to achieve the sensorless interaction force estimation, which is better than traditional direct estimation methods and ESO-based methods in terms of estimation accuracy [12].*
2) *A finite-time observer is designed to estimate the interaction forces with rigorous stability analysis.*

This paper is arranged as follows. The motivation of our work is first explained in Section II. Then, we illustrate the design procedure of the interaction force observer in detail in Section III. Several experiments on a real robot are reported in Section IV. Finally, we conclude this paper in Section V.

II. Motivation

In this section, we discuss the existing interaction force estimation methods and their shortcomings, which motivate our work to cope with these issues.

A. Direct Estimation of $\boldsymbol{\tau}_e$

As a well-established model, the Euler-Lagrange equation [14] has been widely employed to represent the dynamics of robots. Specifically, for a robot manipulator with r-$link$, its dynamic model can be described as

$$\mathbf{M}(\mathbf{q})\ddot{\mathbf{q}} + \mathbf{C}(\mathbf{q}, \dot{\mathbf{q}}) + \mathbf{g}(\mathbf{q}) + \mathbf{f} = \boldsymbol{\tau} + \boldsymbol{\tau}_e, \tag{1}$$

where $\mathbf{q} \in \mathbb{R}^{r\times 1}$, $\dot{\mathbf{q}}$ and $\ddot{\mathbf{q}}$ denote joint position, velocity and acceleration, respectively. $\mathbf{M}(\mathbf{q}) \in \mathbb{R}^{r\times r}$ is a symmetric, positive-definite matrix, $\mathbf{C}(\mathbf{q}, \dot{\mathbf{q}}) \in \mathbb{R}^{r\times 1}$ represents Coriolis and centrifugal terms, $\mathbf{g}(\mathbf{q}) \in \mathbb{R}^{r\times 1}$ denotes gravity, $\mathbf{f} \in \mathbb{R}^{r\times 1}$ represents friction force, $\boldsymbol{\tau}_e \in \mathbb{R}^{r\times 1}$ denotes the interaction force (which will be estimated in this paper without using a torque/force sensor) and $\boldsymbol{\tau} \in \mathbb{R}^{r\times 1}$ denotes joint torque (which is also referred to as control input).

According to (1), the direct estimation can be calculated as

$$\hat{\boldsymbol{\tau}}_e = \mathbf{M}(\mathbf{q})\ddot{\mathbf{q}} + \mathbf{C}(\mathbf{q}, \dot{\mathbf{q}}) + \mathbf{g}(\mathbf{q}) + \mathbf{f} - \boldsymbol{\tau} \tag{2}$$

with $\hat{\boldsymbol{\tau}}_e$ being the estimation of $\boldsymbol{\tau}_e$.

Note that in (2), $\mathbf{q}$, $\dot{\mathbf{q}}$, $\ddot{\mathbf{q}}$ and $\boldsymbol{\tau}$ are needed to calculate the interaction force. However, in practice, only the joint positions $\mathbf{q}$, joint velocity $\dot{\mathbf{q}}$ and $\boldsymbol{\tau}$ can be obtained from the servo drive. A simple solution to estimate $\ddot{\mathbf{q}}$ is to resort to the second order differentiators, which, however, will amplify the noise introduced during the measurement signals.

B. Indirect estimation of $\boldsymbol{\tau}_e$ though traditional extended state observer

In this subsection, we will show the ESO-based interaction force estimation approach and its shortcomings.

Define $\mathbf{x}_1 = \mathbf{q}$, $\mathbf{x}_2 = \dot{\mathbf{q}}$ and $\mathbf{x}_3 = \mathbf{M}(\mathbf{x}_1)^{-1}\boldsymbol{\tau}_e$. The dynamic model in (1) becomes

$$\begin{cases} \dot{\mathbf{x}}_1 = \mathbf{x}_2, \\ \dot{\mathbf{x}}_2 = \mathbf{M}(\mathbf{x}_1)^{-1}\boldsymbol{\tau} + \mathbf{F}(\mathbf{x}_1, \mathbf{x}_2) + \mathbf{x}_3, \end{cases} \tag{3}$$

where the nonlinear function $\mathbf{F}(\mathbf{x}_1, \mathbf{x}_2) \in \mathbb{R}^{r\times 1}$ is defined as

$$\mathbf{F}(\mathbf{x}_1, \mathbf{x}_2) = -\mathbf{M}(\mathbf{x}_1)^{-1}\left(\mathbf{C}(\mathbf{x}_1, \mathbf{x}_2) + \mathbf{g}(\mathbf{x}_1) + \mathbf{f}\right). \tag{4}$$

The standard ESO can be designed to estimate the interaction force, i.e.,

$$\begin{cases} \dot{\mathbf{z}}_1 = \mathbf{z}_2 + \mathbf{k}_1(\mathbf{x}_1 - \mathbf{z}_1), \\ \dot{\mathbf{z}}_2 = \mathbf{M}(\mathbf{x}_1)^{-1}\boldsymbol{\tau} + \mathbf{F}(\mathbf{x}_1, \mathbf{x}_2) + \mathbf{z}_3 + \mathbf{k}_2(\mathbf{x}_1 - \mathbf{z}_1), \\ \dot{\mathbf{z}}_3 = \mathbf{k}_3(\mathbf{x}_1 - \mathbf{z}_1), \\ \hat{\boldsymbol{\tau}}_e = \mathbf{M}(\mathbf{x}_1)\mathbf{z}_3, \end{cases} \tag{5}$$

where $\mathbf{k}_i \in \mathbb{R}^{r\times r}$, $\mathbf{z}_i$, $i = \{1, 2, 3\}$ and $\hat{\boldsymbol{\tau}}_e$ represent design parameters, the estimation of system states $\mathbf{x}_i$ and the estimation of $\boldsymbol{\tau}_e$, respectively.

Denote $\mathbf{e}_1 = \mathbf{x}_1 - \mathbf{z}_1$, $\mathbf{e}_2 = \mathbf{x}_2 - \mathbf{z}_2$, $\mathbf{e}_3 = \mathbf{x}_3 - \mathbf{z}_3$ and $\mathbf{e} = \begin{bmatrix}\mathbf{e}_1^{\mathrm{T}} & \mathbf{e}_2^{\mathrm{T}} & \mathbf{e}_3^{\mathrm{T}}\end{bmatrix}^{\mathrm{T}}$. Combining (3) with (5) yields the error dynamics as

$$\dot{\mathbf{e}} = \mathbf{A}\mathbf{e} + \mathbf{B}\dot{\mathbf{x}}_3 \tag{6}$$

with

$$\mathbf{A} = \begin{bmatrix} -\mathbf{k}_1 & \mathbf{I}_{r\times r} & \mathbf{0}_{r\times r} \\ -\mathbf{k}_2 & \mathbf{0}_{r\times r} & \mathbf{I}_{r\times r} \\ -\mathbf{k}_3 & \mathbf{0}_{r\times r} & \mathbf{0}_{r\times r} \end{bmatrix}, \mathbf{B} = \begin{bmatrix} \mathbf{0}_{r\times r} \\ \mathbf{0}_{r\times r} \\ \mathbf{I}_{r\times r} \end{bmatrix}. \tag{7}$$

Generally, it is trivial to select suitable parameters $\mathbf{k}_i, i = \{1, 2, 3\}$ to ensure that $\mathbf{A}$ is a Hurwitz matrix. Following (6), we have

$$\mathbf{e}(t) = \mathbf{e}^{\mathbf{A}t}\mathbf{e}(0) + \int_0^t \mathbf{e}^{\mathbf{A}(t-\iota)}\mathbf{B}\dot{\mathbf{x}}_3(\iota)d\iota. \tag{8}$$

Note that if $\dot{\mathbf{x}}_3 = \mathbf{0}$, we have $\mathbf{e}(\infty) = \dot{\mathbf{e}}(\infty) = \mathbf{0}$ since $\mathbf{A}$ is a Hurwitz matrix. This implies that ESO can accurately estimate constant or slowly time-varying lumped interaction forces, however, the estimation of non-constant lumped interaction forces is not addressed therein. Suppose that the lumped interaction force $\mathbf{x}_3$ in (3) is non-constant but bounded and with a bounded derivative, i.e., $\|\dot{\mathbf{x}}_3\| < \zeta, \zeta > 0$. Then, (8) can be transformed into

$$\|\mathbf{e}(t)\| \leq \|\mathbf{e}^{\mathbf{A}t}\|\|\mathbf{e}(0)\| + \|\mathbf{A}^{-1}(\mathbf{I} - \mathbf{e}^{\mathbf{A}t})\mathbf{B}\|\zeta. \tag{9}$$

Taking the limit of (9) yields

$$\|\mathbf{e}(\infty)\| \leq \|\mathbf{A}^{-1}\mathbf{B}\|\zeta. \tag{10}$$

Hence, the ESO introduces steady-state estimation errors in the presence of non-constant lumped interaction forces. Please refer to [15] for more detailed discussion on the ESO. This is also the motivation driving us to study a more efficient and accurate observer to estimate time-varying and non-constant interaction forces.

III. Main Results

Before proceeding to present our main results, some key notations and lemma are first introduced.

Notations $\mathbf{x} = \begin{bmatrix}x_1, x_2, \ldots, x_n\end{bmatrix}^{\mathrm{T}}$ denotes a n-dimensional vector with x_i being the ith element of $\mathbf{x}$, where $i = 1, 2, \ldots, n$. $\mathrm{sig}^{\alpha}(\mathbf{x}) = \begin{bmatrix}|x_1|^{\alpha}\mathrm{sign}(x_1), |x_2|^{\alpha}\mathrm{sign}(x_2), \ldots, |x_n|^{\alpha}\mathrm{sign}(x_n)\end{bmatrix}^{\mathrm{T}}$ with $\alpha > 0$. $\mathbf{x}^{\alpha} = \begin{bmatrix}x_1^{\alpha}, x_2^{\alpha}, \ldots, x_n^{\alpha}\end{bmatrix}^{\mathrm{T}}$.

Lemma 1 [16] Let $c, d > 0$. For any $a > 0$, the following inequality holds for $\forall x, y \in \mathbb{R} : |x|^c|y|^d \leq \frac{c}{c+d}a|x|^{c+d} + \frac{d}{c+d}a^{\frac{-c}{d}}|y|^{c+d}$.

A. System Identification

In this subsection, we first build the dynamic model of industrial robots by the parameter identification method so as to facilitate the design of high-order finite-time observers in the next subsection.

During the process of identification, we assume that no external interaction forces are applied to the robot manipulator and therefore $\boldsymbol{\tau}_e$ is set as zero, i.e.,

$$\boldsymbol{\tau}_e = \mathbf{0}. \tag{11}$$

Usually, the friction model of the ith joint is described by [17]

$$f_i = Fc_i \cdot \text{sign}(\dot{q}_i) + Fv_i\dot{q}_i + B_i, \tag{12}$$

where f_i is the ith element of $\mathbf{f}$, Fc_i and Fv_i respectively denote Coulomb and viscous friction coefficients, and B_i is the bias term.

Remark 1: For the friction model, we only consider two conventional dynamics (e.g., Coulomb and viscous friction) since it is effective for our robot. In order to better characterize the friction, as future work, the improved friction models [18], [19], [20] can be used to generalize our results to other robots.

Due to the linearity in the parameters property [14], the inverse dynamic model in (1) can be written as

$$\boldsymbol{\tau} = \mathbf{H}_s(\mathbf{q}, \dot{\mathbf{q}}, \ddot{\mathbf{q}})\boldsymbol{\theta}_s \tag{13}$$

where $\mathbf{H}_s(\mathbf{q}, \dot{\mathbf{q}}, \ddot{\mathbf{q}}) \in \mathbb{R}^{r\times s}$ is called a regressor function and $\boldsymbol{\theta}_s \in \mathbb{R}^{s\times 1}$ represents the standard parameters. For rigid robot manipulators, there are 14 standard parameters for each joint and link, including six components (I_{xxj} I_{xyj} I_{xzj} I_{yyj} I_{yzj} I_{zzj}) of inertia tensor for each link j , first moments (mx_j, my_j, mz_j) of link j, mass m_j, total inertia moment Ia_j and friction parameters Fv_j Fc_j B_j.
In accordance with [21] and [22], we can utilize the column linear dependency of $\mathbf{H}_s$ to regroup the standard parameters and therefore (13) can be rewritten as

$$\boldsymbol{\tau} = \mathbf{H}(\mathbf{q}, \dot{\mathbf{q}}, \ddot{\mathbf{q}})\boldsymbol{\mu}, \tag{14}$$

where $\mathbf{H}(\mathbf{q}, \dot{\mathbf{q}}, \ddot{\mathbf{q}}) \in \mathbb{R}^{r\times p}$ corresponds to a subset of the maximum linear independent columns of $\mathbf{H}_s$ and $\boldsymbol{\mu} \in \mathbb{R}^{p\times 1}$ represents the base parameters.

Remark 2: For rigid robot manipulators, there are 14 standard parameters for each joint and link. If a robot has r joints, the number of standard parameters are $14r$. Hence, $s = 14r$ and $p < s$.

Assuming that we have access to N groups of experimental data $\{\mathbf{H}(\mathbf{q}_t, \dot{\mathbf{q}}_t, \ddot{\mathbf{q}}_t), \boldsymbol{\tau}_\mathbf{t}\}_{t=1}^N$ along an excitation trajectory, we have

$$\mathcal{T} = \mathcal{H}\boldsymbol{\mu}, \tag{15}$$

where $\mathcal{H} = [\mathbf{H}_1{}^{\mathrm{T}}\mathbf{H}_2{}^{\mathrm{T}}\cdots\mathbf{H}_N{}^{\mathrm{T}}]^{\mathrm{T}}$, $\mathcal{T} = [\boldsymbol{\tau}_1{}^{\mathrm{T}}\boldsymbol{\tau}_2{}^{\mathrm{T}}\cdots\boldsymbol{\tau}_N{}^{\mathrm{T}}]^{\mathrm{T}}$. Hence, $\boldsymbol{\mu}$ can be obtained using the least squares estimation [23], [24].

B. Improved Estimation of $\boldsymbol{\tau}_e$ Though high-order finite-time observer

We construct a high-order finite-time observer to estimate the interaction forces, since it provides us with crucial characteristics in interaction force estimation, including estimation accuracy and continuity. In order to design a high-order finite-time observer, the system parameters are required in advance. By importing the identification result, the friction model $\mathbf{f}$ can be extracted. Subsequently, the system parameter matrices $\mathbf{M}(\mathbf{q})$,$\mathbf{C}(\mathbf{q}, \dot{\mathbf{q}})$ and $\mathbf{g}(\mathbf{q})$ are obtained via algebraic sorting as

$$\begin{cases} \mathbf{g}(\mathbf{q}) = \mathbf{H}(\mathbf{q}, \mathbf{0}, \mathbf{0})\boldsymbol{\mu} - \mathbf{f}, \\ \mathbf{C}(\mathbf{q}, \dot{\mathbf{q}}) = \mathbf{H}(\mathbf{q}, \dot{\mathbf{q}}, \mathbf{0})\boldsymbol{\mu} - \mathbf{f} - \mathbf{g}(\mathbf{q}), \\ \mathbf{M}_i(\mathbf{q}) = \mathbf{H}(\mathbf{q}, \mathbf{0}, \mathbf{E}_i)\boldsymbol{\mu} - \mathbf{f} - \mathbf{g}(\mathbf{q}), \end{cases} \tag{16}$$

where $\mathbf{E}_i = [\underbrace{0, \ldots, 0}_{i-1}, 1, \underbrace{0, \ldots, 0}_{r-i}]^{\mathrm{T}}$, $i = 1, \cdots, r$ and $\mathbf{M}_i(\mathbf{q})$ represents the ith column of $\mathbf{M}(\mathbf{q})$.

Now, the HOFTO can be constructed to estimate the interaction force, which is designed as

$$\begin{cases} \dot{\mathbf{z}}_1 = \mathbf{z}_2 + \mathbf{L}_1\text{sig}^{m_2}(\mathbf{x}_1 - \mathbf{z}_1), \\ \dot{\mathbf{z}}_2 = \mathbf{M}(\mathbf{x}_1)^{-1}\boldsymbol{\tau} + \mathbf{F}(\mathbf{x}_1, \mathbf{x}_2) + \mathbf{z}_3, \\ \qquad\quad +\mathbf{L}_2\text{sig}^{m_3}(\mathbf{x}_1 - \mathbf{z}_1), \\ \dot{\mathbf{z}}_3 = \mathbf{z}_4 + \mathbf{L}_3\text{sig}^{m_4}(\mathbf{x}_1 - \mathbf{z}_1), \\ \cdots \\ \dot{\mathbf{z}}_{n+2} = \mathbf{L}_{n+2}\text{sig}^{m_{n+3}}(\mathbf{x}_1 - \mathbf{z}_1), \\ \hat{\boldsymbol{\tau}}_e = \mathbf{M}(\mathbf{x}_1)\mathbf{z}_3, \end{cases} \tag{17}$$

where $\mathbf{z}_1, \mathbf{z}_2, \mathbf{z}_3, \ldots, \mathbf{z}_{n+2}, \hat{\boldsymbol{\tau}}_e$ are estimations corresponding to $\mathbf{x}_1, \mathbf{x}_2, \mathbf{x}_3, \ldots, \mathbf{x}_3^{(n-1)}, \boldsymbol{\tau}_e$. $\mathbf{L}_1, \mathbf{L}_2, \ldots, \mathbf{L}_{n+2} \in \mathbb{R}^{r\times r}$ denote the parameter matrices to be designed. Note that both the numerator and denominator of m_i are odd such that the notation $\mathbf{x}^{m_i} = \text{sig}^{m_i}(\mathbf{x})$ holds, where $m_i = 1 + (i-1)\sigma, \sigma \in (-1/(n+2), 0), i = 1, 2, \ldots, n+3$.

Remark 3: In general, the estimated order is selected according to the physical interaction force model. For instance, one can achieve finite-time stability for the observer by choosing $n = 1, 2$ and 3 for the constant, ramp and parabolic interaction forces, respectively. Similarly, a higher order n can be selected to ensure the estimation accuracy of the more general order interaction forces (e.g., forces with the polynomial types), which however is attained at the cost of an increasing computational burden. In practice, we first consider low-order cases and later increase the order properly if the corresponding estimation is unsatisfactory.

Denote $\bar{\mathbf{e}}_1 = \mathbf{x}_1 - \mathbf{z}_1, \bar{\mathbf{e}}_2 = \mathbf{x}_2 - \mathbf{z}_2, \bar{\mathbf{e}}_3 = \mathbf{x}_3 - \mathbf{z}_3, \cdots, \bar{\mathbf{e}}_{n+2} = \mathbf{x}_3^{(n-1)} - \mathbf{z}_{n+2}$. Combining (3) and (17), we have

$$\begin{cases} \dot{\bar{\mathbf{e}}}_1 = \bar{\mathbf{e}}_2 - \mathbf{L}_1\bar{\mathbf{e}}_1^{m_2}, \\ \dot{\bar{\mathbf{e}}}_2 = \bar{\mathbf{e}}_3 - \mathbf{L}_2\bar{\mathbf{e}}_1^{m_3}, \\ \dot{\bar{\mathbf{e}}}_3 = \bar{\mathbf{e}}_4 - \mathbf{L}_3\bar{\mathbf{e}}_1^{m_4}, \\ \cdots \\ \dot{\bar{\mathbf{e}}}_{n+2} = \mathbf{x}_3^{(n)} - \mathbf{L}_{n+2}\bar{\mathbf{e}}_1^{m_{n+3}}. \end{cases} \tag{18}$$

Redefine $\mathbf{e}_1 = \bar{\mathbf{e}}_1$, $\mathbf{e}_2 = \mathbf{L}_1^{-1}\bar{\mathbf{e}}_2$, $\mathbf{e}_3 = \mathbf{L}_2^{-1}\bar{\mathbf{e}}_3$, $\cdots$, $\mathbf{e}_{n+2} = \mathbf{L}_{n+1}^{-1}\bar{\mathbf{e}}_{n+2}$. (18) can be written as

$$\begin{cases} \dot{\mathbf{e}}_1 = \mathbf{L}_1(\mathbf{e}_2 - \mathbf{e}_1^{m_2}), \\ \dot{\mathbf{e}}_2 = \mathbf{L}_1^{-1}\mathbf{L}_2(\mathbf{e}_3 - \mathbf{e}_1^{m_3}), \\ \dot{\mathbf{e}}_3 = \mathbf{L}_2^{-1}\mathbf{L}_3(\mathbf{e}_4 - \mathbf{e}_1^{m_4}), \\ \cdots \\ \dot{\mathbf{e}}_{n+2} = \mathbf{L}_{n+1}^{-1}\mathbf{x}_3^{(n)} - \mathbf{L}_{n+1}^{-1}\mathbf{L}_{n+2}\mathbf{e}_1^{m_{n+3}}. \end{cases} \tag{19}$$

Denote $\mathbf{K}_1 = \mathbf{L}_1$, $\mathbf{K}_2 = \mathbf{L}_1^{-1}\mathbf{L}_2$, $\mathbf{K}_3 = \mathbf{L}_2^{-1}\mathbf{L}_3$, $\cdots$, $\mathbf{K}_{n+2} = \mathbf{L}_{n+1}^{-1}\mathbf{L}_{n+2}$. Then, we can rewrite (19) as

$$\begin{cases} \dot{\mathbf{e}}_1 = \mathbf{K}_1(\mathbf{e}_2 - \mathbf{e}_1^{m_2}), \\ \dot{\mathbf{e}}_2 = \mathbf{K}_2(\mathbf{e}_3 - \mathbf{e}_1^{m_3}), \\ \dot{\mathbf{e}}_3 = \mathbf{K}_3(\mathbf{e}_4 - \mathbf{e}_1^{m_4}), \\ \cdots \\ \dot{\mathbf{e}}_{n+2} = -\mathbf{K}_{n+2}\mathbf{e}_1^{m_{n+3}} + \mathbf{L}_{n+1}^{-1}\mathbf{x}_3^{(n)}. \end{cases} \tag{20}$$

1) Case 1: estimation of $\mathbf{x}_3$ with time series polynomial form

The following assumption play a key role in introducing the main result.

Assumption 1: The n time derivatives of $\mathbf{x}_{3i}$ exists and satisfies $\mathbf{x}_{3i}^{(n)}(t) = 0$.

Theorem 1: For the robot manipulator system (3) under Assumption 1, if the interaction force observer is designed as (17), then the estimation error will converge to zero in a finite time .

Proof: For the error system (20), if $\mathbf{x}_3^{(n)} = \mathbf{0}$, then we follow the spirit of [25] that there is a Lyapunov function $V(\mathbf{e})$ such that

$$\dot{V}(\mathbf{e}) \leq -\gamma V^{\alpha}(\mathbf{e}), \tag{21}$$

where

$$\gamma > 0, 0 < \alpha < 1,$$

and

$$V(\mathbf{e}) = \sum_{j=1}^{n+2}\sum_{i=1}^{r}\int_{\mathbf{e}_{(j+1)i}^{m_j/m_{j+1}}}^{\mathbf{e}_{(j)i}} \left(s^{\frac{2-m_j}{m_j}} - \mathbf{e}_{(j+1)i}^{\frac{2-m_j}{m_{j+1}}} \right) ds.$$

Hence, we can conclude from (21) that the estimation error will converge to zero in a finite time [25].

2) Case 2: estimation of time-varying interaction forces

The stability of the interaction force observer is introduced by Theorem 2 with satisfying Assumption 2.

Assumption 2: The n time derivatives of external interaction forces $\boldsymbol{\tau}_e(t)$ exist. We can derive that $\mathbf{x}_3$ is continuously differentiable and its high-order derivatives are bounded, i.e., $|\mathbf{x}_{3i}^{(n)}| \leq \kappa_i, i = 1, 2, \ldots, n$.

Remark 4: Assumption 2 needed here is essentially made to guarantee the finite-time convergence of the proposed observer with rigorous stability analysis. From a theoretical point of view, the proposed observer is finite-time convergent. As for the susceptibility of the closed-loop system to noise, we do not consider it in this paper. To our knowledge, no results have been reported on this topic. However, this problem deserves to be studied in the future.

Theorem 2: For the robot manipulator system (3) under Assumption 2, if the interaction force observer is designed as (17), then the estimation value will converge to a bounded region in a finite time .

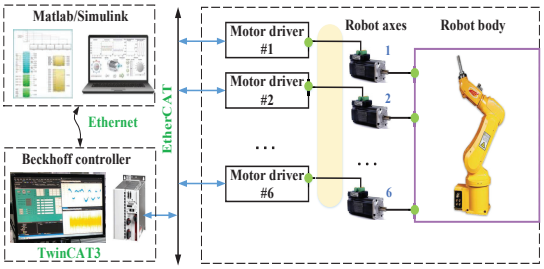

(a)

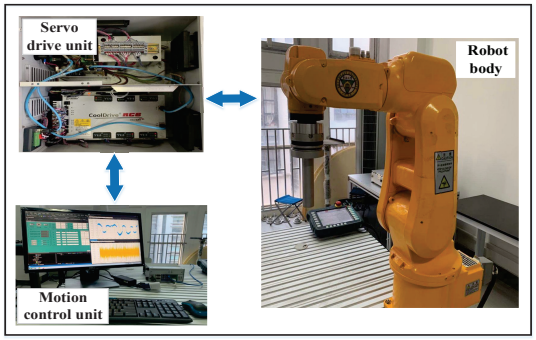

(b)

Fig. 1. Experiment setup. (a): The diagram of the robotics system. (b): Hardware architecture of the robot.

Proof: Define $\mathbf{H}_{i,j}(\mathbf{e}_{j+1}, \mathbf{e}_j) = [\mathbf{e}_{j+1}^{\frac{1}{j\sigma+1}}]^{i\sigma+1} - [\mathbf{e}_j^{\frac{1}{(j-1)\sigma+1}}]^{i\sigma+1}$. Then, we have $\sum_{j=1}^{i}\mathbf{H}_{i,j} = \mathbf{e}_{i+1} - \mathbf{e}_1^{m_{i+1}}, i = 1, \ldots, n+2$. Hence, the (20) can be rewritten as

$$\begin{cases} \dot{\mathbf{e}}_1 = \mathbf{K}_1\mathbf{H}_{1,1}, \\ \dot{\mathbf{e}}_2 = \mathbf{K}_2(\mathbf{H}_{2,2} + \mathbf{H}_{2,1}), \\ \dot{\mathbf{e}}_3 = \mathbf{K}_3(\mathbf{H}_{3,3} + \mathbf{H}_{3,2} + \mathbf{H}_{3,1}), \\ \cdots \\ \dot{\mathbf{e}}_{n+2} = -\mathbf{K}_{n+2}(\mathbf{H}_{n+2,n+2} + \cdots + \mathbf{H}_{n+2,1}) \\ \qquad\quad +\mathbf{L}_{n+1}^{-1}\mathbf{x}_3^{(n)}. \end{cases} \tag{22}$$

Here, we can construct the same Lyapunov function shown in (21). Then, the derivative of $V(\mathbf{e})$ along system (22) can be written

$$\begin{aligned} \dot{V}|_{(22)} \leq & -\sum_{j=1}^{n+2}\sum_{i=1}^{r}|\mathbf{e}_{(j+1)i} - \mathbf{e}_{(j)i}^{m_{j+1}/m_j}|^{\frac{2+\sigma}{m_{j+1}}} \\ & + \sum_{i=1}^{r}\frac{\partial V(\mathbf{e})}{\partial \mathbf{e}_{(n+2)i}}\mathbf{L}_{(n+1)i}^{-1}\mathbf{x}_{3i}^{(n)} \\ \leq & -\gamma V^{\alpha}(\mathbf{e}) + \sum_{i=1}^{r}\frac{\partial V(\mathbf{e})}{\partial \mathbf{e}_{(n+2)i}}\mathbf{L}_{(n+1)i}^{-1}\kappa_i, \end{aligned} \tag{23}$$

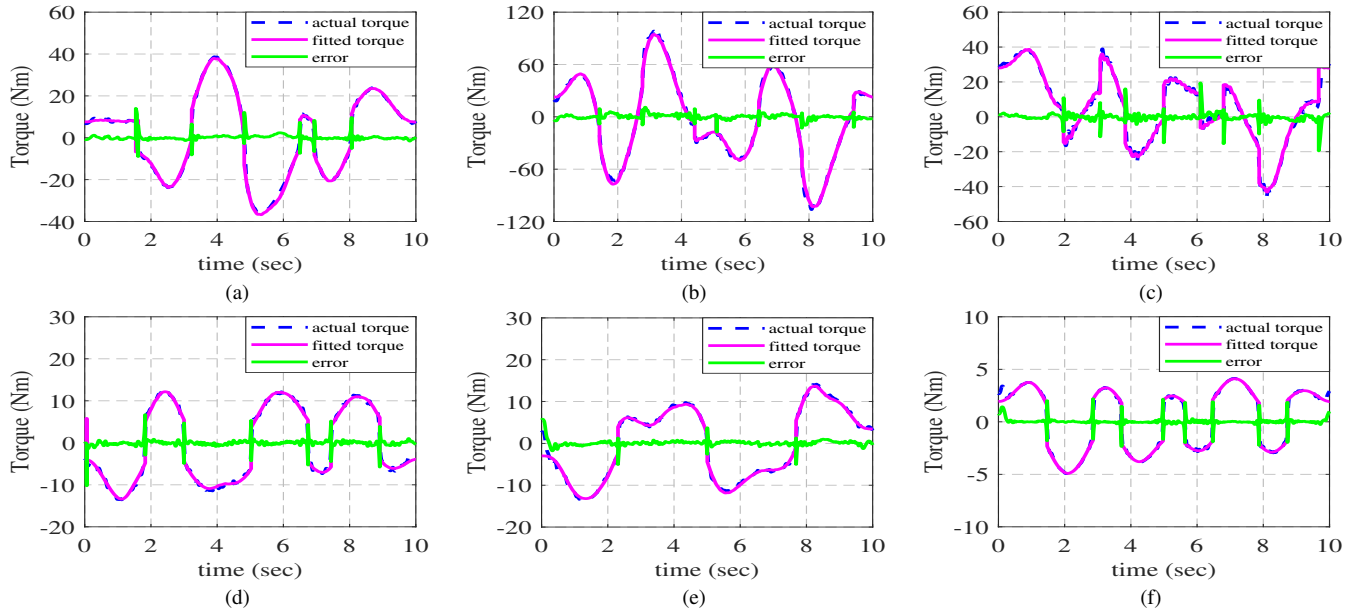

Fig. 2. Comparison between the measured and estimated torque. $(a)-(f)$ correspond to the 1st−6th joints, where the blue dashed, red solid and green solid curves depict the measured torque, estimated torque and the corresponding torque errors, respectively.

where

$$\sum_{i=1}^{r}\frac{\partial V(\mathbf{e})}{\partial \mathbf{e}_{(n+2)i}} = \sum_{i=1}^{r}\mathbf{e}_{(n+2)i}^{(2-m_{n+2})/m_{n+2}} - \sum_{i=1}^{r}\frac{2-m_{n+1}}{m_{n+2}}\mathbf{e}_{(n+2)i}^{\frac{2-m_{n+1}}{m_{n+2}}-1}\mathbf{e}_{(n+1)i} + \sum_{i=1}^{r}\frac{2-m_{n+1}}{m_{n+2}}\mathbf{e}_{(n+2)i}^{\frac{2-m_{n+1}}{m_{n+2}}-1}\mathbf{e}_{(n+2)i}^{\frac{m_{n+1}}{m_{n+2}}}. \tag{24}$$

Considering

$$|\mathbf{e}_{(n+1)i}-\mathbf{e}_{(n+2)i}^{\frac{m_{n+1}}{m_{n+2}}}| \le b|\mathbf{e}_{(n+1)i}^{\frac{m_{n+2}}{m_{n+1}}}-\mathbf{e}_{(n+2)i}|^{\frac{m_{n+1}}{m_{n+2}}} + b|\mathbf{e}_{(n+1)i}^{\frac{m_{n+2}}{m_{n+1}}}-\mathbf{e}_{(n+2)i}||\mathbf{e}_{(n+2)i}|^{\frac{m_{n+1}}{m_{n+2}}-1}, \tag{25}$$

with $b>0$ being a constant, then we have

$$|\mathbf{e}_{(n+2)i}^{\frac{2-m_{n+1}}{m_{n+2}}-1}(\mathbf{e}_{(n+1)i}-\mathbf{e}_{(n+2)i}^{\frac{m_{n+1}}{m_{n+2}}})| \le b|\mathbf{e}_{(n+2)i}|^{\frac{2-m_{n+1}}{m_{n+2}}-1}|\mathbf{e}_{(n+1)i}^{\frac{m_{n+2}}{m_{n+1}}}-\mathbf{e}_{(n+2)i}|^{\frac{m_{n+1}}{m_{n+2}}} + b|\mathbf{e}_{(n+2)i}|^{\frac{2-m_{n+2}+\sigma}{m_{n+2}}}|\mathbf{e}_{(n+1)i}^{\frac{m_{n+2}}{m_{n+1}}}-\mathbf{e}_{(n+2)i}|. \tag{26}$$

Following Lemma 1, we have

$$b|\mathbf{e}_{(n+2)i}|^{\frac{2-m_{n+1}}{m_{n+2}}-1}|\mathbf{e}_{(n+1)i}^{\frac{m_{n+2}}{m_{n+1}}}-\mathbf{e}_{(n+2)i}|^{\frac{m_{n+1}}{m_{n+2}}} \le b_1|\mathbf{e}_{(n+2)i}|^{\frac{2-m_{n+2}}{m_{n+2}}} + b_2|\mathbf{e}_{(n+1)i}^{\frac{m_{n+2}}{m_{n+1}}}-\mathbf{e}_{(n+2)i}|^{\frac{2-m_{n+2}}{m_{n+2}}} \tag{27}$$

and

$$b|\mathbf{e}_{(n+2)i}|^{\frac{2-m_{n+2}+\sigma}{m_{n+2}}}|\mathbf{e}_{(n+1)i}^{\frac{m_{n+2}}{m_{n+1}}}-\mathbf{e}_{(n+2)i}| \le b_3|\mathbf{e}_{(n+2)i}|^{\frac{2+\sigma}{m_{n+2}}} + b_4|\mathbf{e}_{(n+1)i}^{\frac{m_{n+2}}{m_{n+1}}}-\mathbf{e}_{(n+2)i}|^{\frac{2+\sigma}{m_{n+2}}} \tag{28}$$

with $b_1 = b\frac{2-m_{n+1}-m_{n+2}}{2-m_{n+2}}$, $b_2 = b\frac{m_{n+1}}{2-m_{n+2}}$, $b_3 = b\frac{2-m_{n+2}+\sigma}{2+\sigma}$ and $b_4 = b\frac{m_{n+2}}{2+\sigma}$.

Combining (27) and (28), (26) can be rewritten as

$$|\mathbf{e}_{(n+2)i}^{\frac{2-m_{n+1}}{m_{n+2}}-1}(\mathbf{e}_{(n+1)i}-\mathbf{e}_{(n+2)i}^{\frac{m_{n+1}}{m_{n+2}}})| \le b_1|\mathbf{e}_{(n+2)i}|^{\frac{2-m_{n+2}}{m_{n+2}}} + b_3|\mathbf{e}_{(n+2)i}|^{\frac{2+\sigma}{m_{n+2}}} + b_2|\mathbf{e}_{(n+1)i}^{\frac{m_{n+2}}{m_{n+1}}}-\mathbf{e}_{(n+2)i}|^{\frac{2-m_{n+2}}{m_{n+2}}} + b_4|\mathbf{e}_{(n+1)i}^{\frac{m_{n+2}}{m_{n+1}}}-\mathbf{e}_{(n+2)i}|^{\frac{2+\sigma}{m_{n+2}}}. \tag{29}$$

Hence, (24) can be rewritten as

$$\sum_{i=1}^{r}\frac{\partial V(\mathbf{e})}{\partial \mathbf{e}_{(n+2)i}} \le \sum_{i=1}^{r}b_5|\mathbf{e}_{(n+2)i}|^{\frac{2-m_{n+2}}{m_{n+2}}} + \sum_{i=1}^{r}b_6|\mathbf{e}_{(n+2)i}|^{\frac{2+\sigma}{m_{n+2}}} + \sum_{i=1}^{r}b_7|\mathbf{e}_{(n+1)i}^{\frac{m_{n+2}}{m_{n+1}}}-\mathbf{e}_{(n+2)i}|^{\frac{2-m_{n+2}}{m_{n+2}}} + \sum_{i=1}^{r}b_8|\mathbf{e}_{(n+1)i}^{\frac{m_{n+2}}{m_{n+1}}}-\mathbf{e}_{(n+2)i}|^{\frac{2+\sigma}{m_{n+2}}} \le \sum_{i=1}^{r}b_9|\mathbf{e}_{(n+2)i}|^{\frac{2+\sigma}{m_{n+2}}} + rb_5\frac{m_{n+3}}{2+\sigma} + \sum_{i=1}^{r}b_{10}|\mathbf{e}_{(n+1)i}^{\frac{m_{n+2}}{m_{n+1}}}-\mathbf{e}_{(n+2)i}|^{\frac{2+\sigma}{m_{n+2}}} + rb_7\frac{m_{n+3}}{2+\sigma} \tag{30}$$

with $b_5 = \frac{2-m_{n+1}}{m_{n+2}}b_1+1$, $b_6 = \frac{2-m_{n+1}}{m_{n+2}}b_3$, $b_7 = \frac{2-m_{n+1}}{m_{n+2}}b_2$, $b_8 = \frac{2-m_{n+1}}{m_{n+2}}b_4$, $b_9 = b_5\frac{2-m_{n+2}}{2+\sigma}+b_6$ and $b_{10} = b_7\frac{2-m_{n+2}}{2+\sigma}+b_8$.

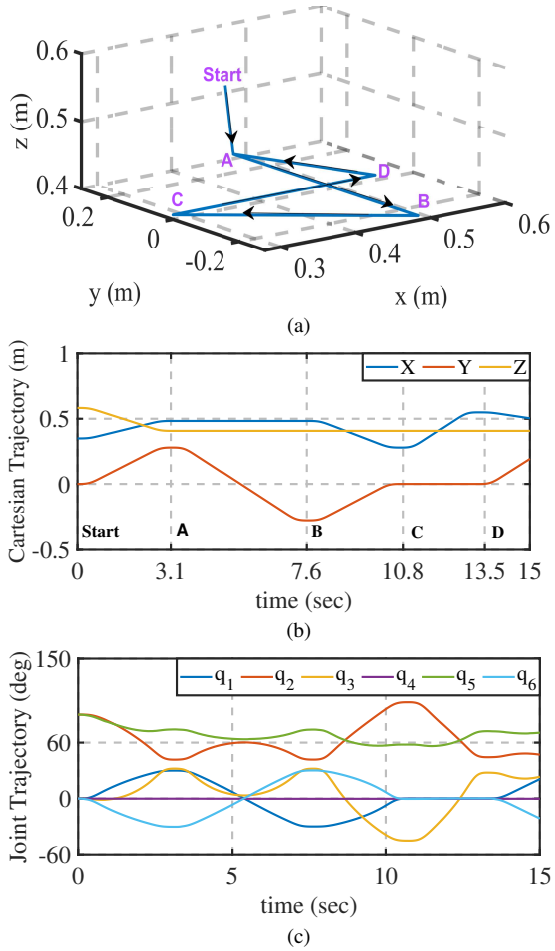

Fig. 3. (a) shows the 3-D motion trajectory. (b)−(c) correspond to trajectories in Cartesian space and joint space, respectively. *Start*, A, B, C and D separately mark the starting and desired points.

Combining (30), (23) can be written as

$$\begin{aligned}\dot{V}|_{(22)} &\leq -\gamma V^{\alpha}(\mathbf{e}) + \sum_{i=1}^{r} \frac{\partial V(\mathbf{e})}{\partial \mathbf{e}_{(n+2)i}} \mathbf{L}^{-1}_{(n+1)i} \kappa_i \\ &\leq -\gamma V^{\alpha}(\mathbf{e}) + \sum_{i=1}^{r} b_9 \mathbf{L}^{-1}_{(n+1)i} \kappa_i |\mathbf{e}_{(n+2)i}|^{\frac{2+\sigma}{m_{n+2}}} \\ &\quad + \sum_{i=1}^{r} b_{10} \mathbf{L}^{-1}_{(n+1)i} \kappa_i |\mathbf{e}^{\frac{m_{n+2}}{m_{n+1}}}_{(n+1)i} - \mathbf{e}_{(n+2)i}|^{\frac{2+\sigma}{m_{n+2}}} \\ &\quad + \sum_{i=1}^{r} \mathbf{L}^{-1}_{(n+1)i} \kappa_i b_5 \frac{m_{n+3}}{2+\sigma} + \sum_{i=1}^{r} \mathbf{L}^{-1}_{(n+1)i} \kappa_i b_7 \frac{m_{n+3}}{2+\sigma} \\ &\leq -\gamma V^{\alpha}(\mathbf{e}) + \gamma_1 V^{\alpha}(\mathbf{e}) + \Theta = -\rho V^{\alpha}(\mathbf{e}) + \Theta \end{aligned} \tag{31}$$

where $\rho = \gamma - \gamma_1 > 0$, $\gamma_1 = \max\{b_9 \mathbf{L}^{-1}_{(n+1)i} \kappa_i, b_{10} \mathbf{L}^{-1}_{(n+1)i} \kappa_i\}$,$i = 1, 2, \ldots, r$ and $\Theta > 0$ are constant.

According to (31), we can conclude that the estimation value will converge to a bounded region Ω in a finite time, where

$$\Omega = \left\{ \mathbf{e}_i \mid V(\mathbf{e}) \leq (\frac{\Theta}{\rho})^{\frac{1}{\alpha}}, i = 1, 2, \ldots, n+2 \right\}. \tag{32}$$

This completes the proof. ■

Remark 5: Generally, the estimation error of HOFTO can be reduced by increasing gain-related parameters $\mathbf{L}_i$,$i = 1, 2, \ldots, n+2$, however, it is noted that too large $\mathbf{L}_i$ will bring some other issues, such as noise amplification and overshoot. Therefore, in this case, we can also adjust the fractional power α to reduce the estimation error, which outperforms the ESO.

Remark 6: The HOFTO exhibits the advantage over the ESO [12] in terms of estimation accuracy. Unlike the ESO that can only accurately estimate constant or slowly time-varying interaction forces, the estimation accuracy for the fast time-varying interaction forces is not as high as the HOFTO.

Remark 7: In (17), if all of fractional power terms m_2, m_3 and m_4 are equal to 1, and meanwhile if $\mathbf{z}_4 = \mathbf{0}, \ldots, \mathbf{z}_{n+2} = \mathbf{0}$, the HOFTO in (17) will be equivalent to the ESO. The advantage of HOFTO over ESO is clarified in non-smooth control, please refer to, e.g., [26], [27]. In addition, if $\mathbf{z}_4 = \mathbf{0}, \ldots, \mathbf{z}_{n+2} = \mathbf{0}$, $m_2 = \frac{1}{2}$, $m_3 = \frac{1}{2}$, and $m_4 = 0$, the HOFTO in (17) will be equivalent to the STA observer.

IV. Experimental Evaluations

In this section, a series of evaluations on a real robot manipulator (ER3A robot, made by Efort Intelligent Equipment Co.,Ltd) are reported to show the performance of our approach. The robotic system is depicted in Fig. 1, which consists of a motion control unit, a servo drive unit and a basic machine unit. The motion control unit is implemented by a Beckhoff controller and developed in the Matlab/Simulink environment through a model-based design (MBD) method. The servo drive unit is governed by a motion controller using the EtherCAT protocol. The basic machine unit is composed of six rotational joints and equipped with a 6-D force/torque sensor attached at the end-effector of the robot.

Following the dynamics identification approach in Section III-A, we can estimate the relevant dynamics model parameters, as listed in Table I, where all units are in SI units. The performance of the identified dynamics model on an excitation trajectory is shown in Fig. 2, where the blue curves denote the real torque inputs over the course of executing the excitation trajectory while the red curves correspond to the estimated torque with the identified dynamics model. We can see from the error curves (green curves) that the identification is satisfactory.

A. Evaluations of Force Estimation

In order to evaluate the accuracy of force estimation, we consider a tracking task where the X-, Y- and Z- components of the desired Cartesian trajectory is plotted Fig. 3(b) and the corresponding 3-D trajectory is shown in Fig. 3(a). Here, the corresponding desired joint trajectory is determined by using the Jacobin-based inverse kinematics, as shown in Fig. 3(c). Note that the most challenging situation for interaction force estimation is when some joints are unchanged or at ultra-low speeds. In Fig. 3(c), the 4th joint is almost unaltered, which leads to a challenging situation for interaction force estimation.

For the sake of comparison, we evaluate the traditional ESO-based estimation method whose gain parameters are set as $\mathbf{k}_1 = \text{diag}\{8, 8, 5, 5, 5, 5\}$, $\mathbf{k}_2 = \text{diag}\{50, 50, 40, 40, 40, 40\}$

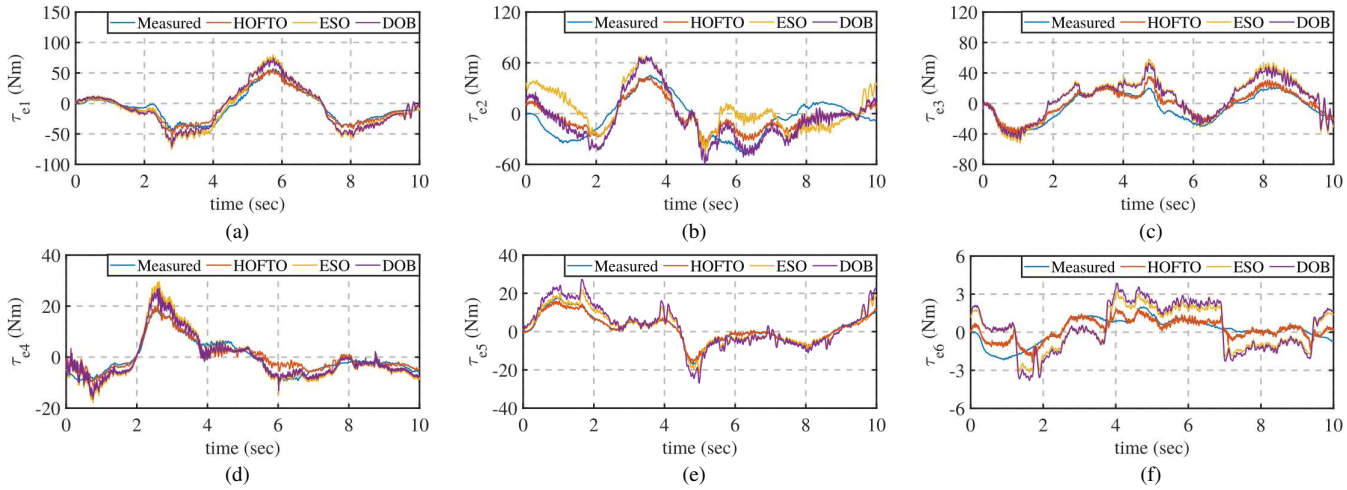

Fig. 4. Comparison among the HOFTO-based (red curve) method, the ESO-based (yellow curve) method and the DOB (purple curve) method. $(a)-(f)$ correspond to the 1st$-$6th joints, respectively. The blue curves depict the real measured external torque.

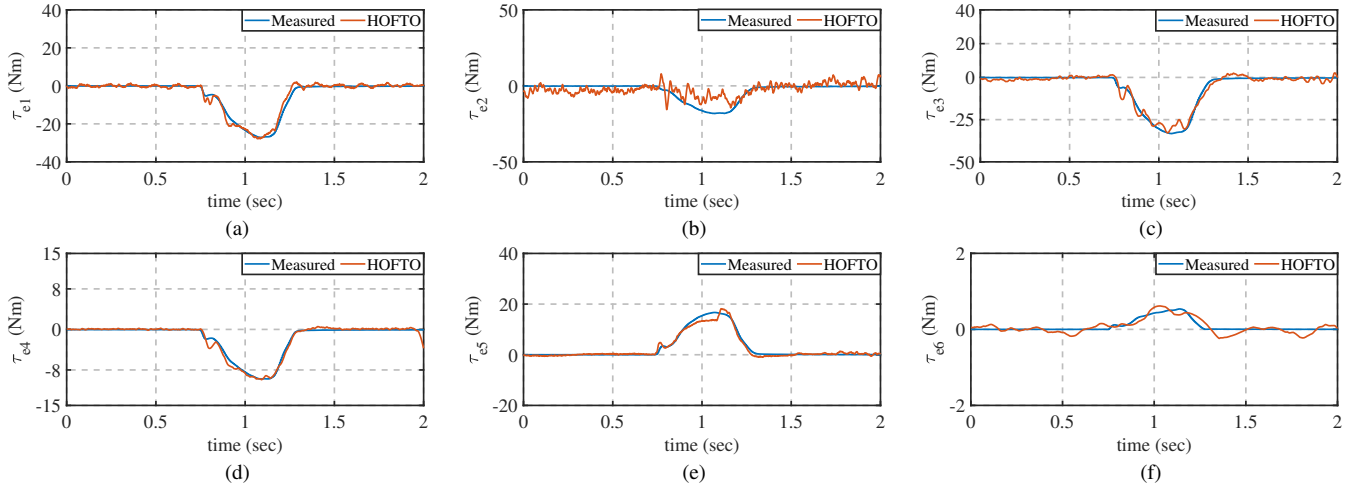

Fig. 5. The estimated and measured interaction force in collision detection. (a)$-$(f) correspond to the 1st$-$6th joints.

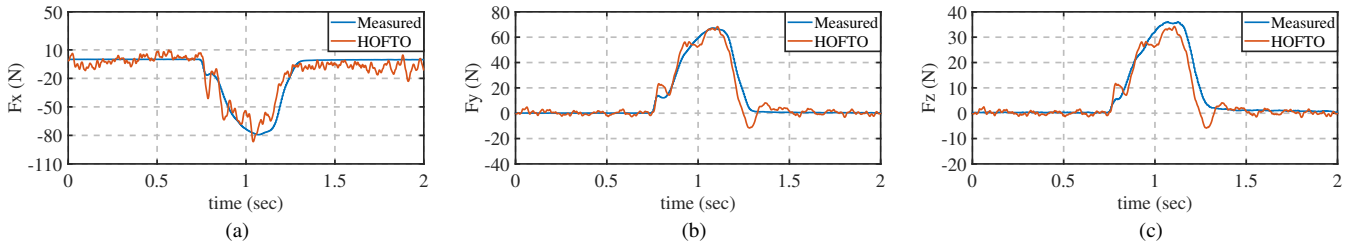

Fig. 6. The estimated and measured interaction force in collision detection. (a)$-$(c) correspond to the X-, Y- and Z- directions in Cartesian space.

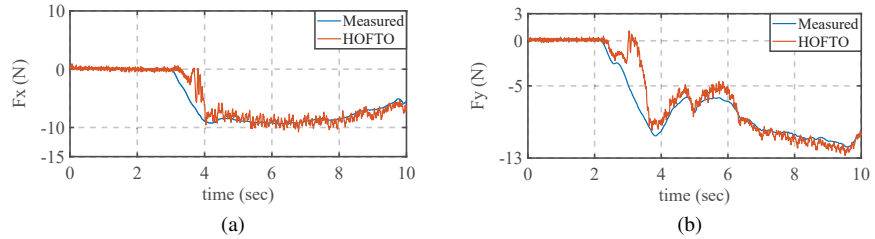

Fig. 7. (a) and (b) correspond to traction tracking along the X- and Y- directions, respectively.

TABLE I
IDENTIFICATION RESULTS

item	value	item	value	item	value	item	value
μ_1	0.853	μ_{17}	0.284	μ_{33}	0.119	μ_{49}	-0.000
μ_2	24.157	μ_{18}	-0.197	μ_{34}	5.412	μ_{50}	0.010
μ_3	7.535	μ_{19}	-0.273	μ_{35}	4.913	μ_{51}	-0.001
μ_4	0.056	μ_{20}	0.732	μ_{36}	-0.025	μ_{52}	0.002
μ_5	0.346	μ_{21}	1.910	μ_{37}	0.079	μ_{53}	0.003
μ_6	0.593	μ_{22}	1.274	μ_{38}	0.032	μ_{54}	-0.001
μ_7	0.162	μ_{23}	13.127	μ_{39}	0.061	μ_{55}	0.021
μ_8	-0.267	μ_{24}	9.924	μ_{40}	0.087	μ_{56}	0.573
μ_9	-0.220	μ_{25}	-0.445	μ_{41}	0.038	μ_{57}	1.946
μ_{10}	2.028	μ_{26}	0.119	μ_{42}	-0.021	μ_{58}	-0.006
μ_{11}	0.845	μ_{27}	-0.038	μ_{43}	0.181	μ_{59}	-5.136
μ_{12}	59.052	μ_{28}	0.110	μ_{44}	0.060	μ_{60}	-13.643
μ_{13}	8.975	μ_{29}	0.061	μ_{45}	6.716	μ_{61}	0.053
μ_{14}	3.492	μ_{30}	0.044	μ_{46}	3.230	μ_{62}	-0.492
μ_{15}	-0.181	μ_{31}	-0.023	μ_{47}	0.054	μ_{63}	-1.143
μ_{16}	0.015	μ_{32}	0.096	μ_{48}	-0.008	μ_{64}	-0.013

TABLE II
PERFORMANCE INDICES UNDER THREE ESTIMATION APPROACHES

	$\boldsymbol{\tau}_{e1}$			$\boldsymbol{\tau}_{e2}$			$\boldsymbol{\tau}_{e3}$		
	Offset	MA	RMS	Offset	MA	RMS	Offset	MA	RMS
HOFTO	0.6566	19.0628	5.6758	1.4586	30.0325	13.7747	4.5513	29.8924	6.9009
ESO	2.0557	31.0833	10.7413	10.2418	60.2324	27.800	11.6811	39.0532	16.4946
DOB	1.8935	28.6627	10.6633	7.609	58.3107	20.1128	11.0636	34.5772	14.8554
	$\boldsymbol{\tau}_{e4}$			$\boldsymbol{\tau}_{e5}$			$\boldsymbol{\tau}_{e6}$		
	Offset	MA	RMS	Offset	MA	RMS	Offset	MA	RMS
HOFTO	0.5386	9.4659	2.8030	0.0239	3.4266	0.9214	0.0885	2.1013	0.5057
ESO	1.1106	11.5670	4.3130	0.6496	9.1514	2.7173	0.1063	2.5020	1.3726
DOB	0.8419	10.1855	3.6928	1.1858	14.3877	4.3777	0.1560	2.9912	1.6311

and $\mathbf{k}_3 = \text{diag}\{300, 300, 200, 200, 200, 200\}$. In addition, the disturbance-observer-based (DOB) method in [10] is also evaluated. Meanwhile, we choose the 4th-order HOFTO design, namely, $n = 2$, whose gain parameters for the proposed HOFTO-based estimation scheme are defined as $\mathbf{L}_1 = \text{diag}\{22.3607, 22.3607, 21.6265, 20.8090, 20.8090, 20.8090\}$, $\mathbf{L}_2 = \text{diag}\{22.101, 22.101, 21.1419, 20.083, 20.083, 20.083\}$, $\mathbf{L}_3 = \text{diag}\{30, 30, 28.0624, 25.9808, 25.9808, 25.9808\}$ and $\mathbf{L}_4 = \text{diag}\{440, 440, 385, 330, 330, 330\}$. Note that the parameter adjustment is mainly based on the recursive selection scheme introduced in [28] and supplemented by the trial-and-error method.

The estimated interaction forces by using the HOFTO, the ESO-based and the DOB methods are shown in Fig. 4, where the real measured torque by using a torque/force sensor is provided as the baseline. It can be seen that the HOFTO method indeed has a more precise estimation compared to ESO-based and DOB approaches. Furthermore, to quantitatively assess our method, the performance indices including the offset value defined as the absolute of the mean value of estimating errors, the maximum absolute (MA) value representing the maximum of absolute value of a sequence of data and the root-mean-squared (RMS) value denoting the square root of the average

of squares of a set of data are taken into account. The quantitative evaluations are summarized in Table II, showing that HOFTO improves the estimation precision over ESO and DOB significantly. Note that, due to unmodeled dynamics and measurement noise, the proposed method still brings estimation errors, but these errors are trivial for human-robot interaction applications.

B. Evaluations of Collision Detection

Collision detection is a very common task in industrial scenarios. In the event of a collision, it is often required to detect external contact forces. In our experiment, we block the end-effector of a robot when it collides with an obstacle.

During the collision, the response curves of the interaction force estimation in joint space and Cartesian space are shown in Fig. 5 and Fig. 6, respectively, from which we can observe that the proposed estimation strategy detects the external force effectively.

C. Sensorless Drag Control

Impedance control is widely used in human-robot interaction scenarios [29], which can be expressed as

$$\mathbf{M}_a\ddot{\mathbf{X}}_d + \mathbf{B}_a\dot{\mathbf{X}}_d + \mathbf{K}_a\mathbf{X}_d = \mathbf{F}_e - \mathbf{F}_d, \tag{33}$$

where $\mathbf{X}_d$ and $\mathbf{F}_d$ represent the desired position in Cartesian space and the contact force with the end-effector, respectively. $\mathbf{M}_a$, $\mathbf{B}_a$, and $\mathbf{K}_a$ denote the inertia matrix, damping matrix, and stiffness matrix of the target impedance model, respectively, and $\mathbf{F}_e$ is the interaction force.

With the estimated interaction forces, we realize the sensorless drag and teaching function by setting $\mathbf{K}_a = \mathrm{diag}\{\mathbf{0}_{1\times 6}\}$ and $\mathbf{F}_d = \mathbf{0}_{6\times 1}$ in (33), giving

$$\mathbf{M}_a\ddot{\mathbf{X}}_d + \mathbf{B}_a\dot{\mathbf{X}}_d = (\mathbf{J}^{\mathrm{T}})^{-1}\hat{\boldsymbol{\tau}}_e \tag{34}$$

with $\mathbf{J}$ being the jacobian matrix. In the procedure of traction, the estimated contact forces along the X- and Y- directions are shown in Fig. 7 (a) and (b), respectively. Note that the chattering shown in Fig. 7 results from two main factors. First, the proposed HOFTO is essentially a non-smooth and nonlinear observer, where the chattering is caused by the parameter adjustment, especially the fractional power term. When fractional power terms are 0, the proposed observer will become non-continuous as the function $\mathrm{sig}(\cdot)$ in our observer degrades into the switching function $\mathrm{sign}(\cdot)$. In this case, chattering is the largest. When fractional power terms are 1, the proposed observer will become linearly continuous. In this case, the chattering can be avoided, but the finte time convergence can not be guaranteed. Therefore, in our experiments the fractional power term is set as $(0, 1)$ as a trade-off between chattering and the finite time convergence. Second, measurement noise is a chattering-producing factor that cannot be ignored.

V. Conclusion

Interaction force estimation has been viewed as a vital research line in the context of force control. This paper has presented an observer for estimating the interaction forces applied to industrial robot manipulators. Following the procedure in this paper, a finite-time convergent HOFTO has been established. Through several evaluations on a real robotic manipulator, we demonstrated that the proposed nonlinear HOFTO is capable of estimating the interaction forces more precisely than ESO and performs well in various applications including collision detection and impedance control.

References

[1] B. Siciliano and L. Villani, *Robot force control*. Springer Science & Business Media, 2012.

[2] S. Zhang, S. Wang, F. Jing, and M. Tan, "A sensorless hand guiding scheme based on model identification and control for industrial robot," *IEEE Transactions on Industrial Informatics*, vol. 15, no. 9, pp. 5204–5213, 2019.

[3] P. Cao, Y. Gan, and X. Dai, "Model-based sensorless robot collision detection under model uncertainties with a fast dynamics identification," *International Journal of Advanced Robotic Systems*, vol. 16, no. 3, pp. 1–15, 2019.

[4] E. Magrini, F. Flacco, and A. De Luca, "Estimation of contact forces using a virtual force sensor," in *Conference on Intelligent Robots and Systems*, pp. 2126–2133, 2014.

[5] A. Wahrburg, J. Bös, K. D. Listmann, F. Dai, B. Matthias, and H. Ding, "Motor-current-based estimation of cartesian contact forces and torques for robotic manipulators and its application to force control," *IEEE Transactions on Automation Science and Engineering*, vol. 15, no. 2, pp. 879–886, 2017.

[6] C. Yang, G. Peng, L. Cheng, J. Na, and Z. Li, "Force sensorless admittance control for teleoperation of uncertain robot manipulator using neural networks," *IEEE Transactions on Systems, Man, and Cybernetics: Systems*, DOI 10.1109/TSMC.2019.2920870, pp. 1–11, 2019.

[7] S. Haddadin, A. De Luca, and A. Albu-Schäffer, "Robot collisions: A survey on detection, isolation, and identification," *IEEE Transactions on Robotics*, vol. 33, no. 6, pp. 1292–1312, 2017.

[8] J. Na, B. Jing, Y. Huang, G. Gao, and C. Zhang, "Unknown system dynamics estimator for motion control of nonlinear robotic systems," *IEEE Transactions on Industrial Electronics*, vol. 67, no. 5, pp. 3850–3859, 2019.

[9] K. S. Eom, I. H. Suh, W. K. Chung, and S.-R. Oh, "Disturbance observer based force control of robot manipulator without force sensor," in *Conference on Robotics and Automation*, vol. 4, pp. 3012–3017, 1998.

[10] E. Sariyildiz and K. Ohnishi, "On the explicit robust force control via disturbance observer," *IEEE Transactions on Industrial Electronics*, vol. 62, no. 3, pp. 1581–1589, 2014.

[11] E. Sariyildiz and K. Ohnishi, "Stability and robustness of disturbance-observer-based motion control systems," *IEEE Transactions on Industrial Electronics*, vol. 62, no. 1, pp. 414–422, 2014.

[12] G. Sebastian, Z. Li, V. Crocher, D. Kremers, Y. Tan, and D. Oetomo, "Interaction force estimation using extended state observers: An application to impedance-based assistive and rehabilitation robotics," *IEEE Robotics and Automation Letters*, vol. 4, no. 2, pp. 1156–1161, 2019.

[13] G. Garofalo, N. Mansfeld, J. Jankowski, and C. Ott, "Sliding mode momentum observers for estimation of external torques and joint acceleration," in *Conference on Robotics and Automation*, pp. 6117–6123, 2019.

[14] M. W. Spong, "On the robust control of robot manipulators," *IEEE Transactions on Automatic Control*, vol. 37, no. 11, pp. 1782–1786, 1992.

[15] S. Li, J. Yang, W.-H. Chen, and X. Chen, *Disturbance observer-based control: methods and applications*. CRC press, 2014.

[16] C. Qian and W. Lin, "A continuous feedback approach to global strong stabilization of nonlinear systems," *IEEE Transactions on Automatic Control*, vol. 46, no. 7, pp. 1061–1079, 2001.

[17] Y. Han, J. Wu, C. Liu, and Z. Xiong, "An iterative approach for accurate dynamic model identification of industrial robots," *IEEE Transactions on Robotics*, vol. 36, no. 5, pp. 1577–1594, 2020.

[18] L. Simoni, M. Beschi, G. Legnani, and A. Visioli, "Friction modeling with temperature effects for industrial robot manipulators," in *Conference on Intelligent Robots and Systems*, pp. 3524–3529, 2015.
[19] A. Wahrburg, S. Klose, D. Clever, T. Groth, S. Moberg, J. Styrud, and H. Ding, "Modeling speed-, load-, and position-dependent friction effects in strain wave gears," in *Conference on Robotics and Automation*, pp. 2095–2102, 2018.
[20] S. Wolf and M. Iskandar, "Extending a dynamic friction model with nonlinear viscous and thermal dependency for a motor and harmonic drive gear," in *Conference on Robotics and Automation*, pp. 783–790, 2018.
[21] M. Gautier and W. Khalil, "Direct calculation of minimum set of inertial parameters of serial robots," *IEEE Transactions on Robotics and Automation*, vol. 6, no. 3, pp. 368–373, 1990.
[22] H. Mayeda, K. Yoshida, and K. Osuka, "Base parameters of manipulator dynamic models," in *Conference on Robotics and Automation*, pp. 1367–1372, 1988.
[23] J. Wu, J. Wang, and Z. You, "An overview of dynamic parameter identification of robots," *Robotics and Computer-Integrated Manufacturing*, vol. 26, no. 5, pp. 414–419, 2010.
[24] J. Jin and N. Gans, "Parameter identification for industrial robots with a fast and robust trajectory design approach," *Robotics and Computer-Integrated Manufacturing*, vol. 31, pp. 21–29, 2015.
[25] H. Du, C. Qian, S. Yang, and S. Li, "Recursive design of finite-time convergent observers for a class of time-varying nonlinear systems," *Automatica*, vol. 49, no. 2, pp. 601–609, 2013.
[26] C. Zhang, Y. Yan, C. Wen, J. Yang, and H. Yu, "A nonsmooth composite control design framework for nonlinear systems with mismatched disturbances: Algorithms and experimental tests," *IEEE Transactions on Industrial Electronics*, vol. 65, no. 11, pp. 8828–8839, 2018.
[27] P. Lin, C. Zhang, J. Wang, C. Jin, and P. Wang, "On autonomous large-signal stabilization for islanded multibus dc microgrids: A uniform nonsmooth control scheme," *IEEE Transactions on Industrial Electronics*, vol. 67, no. 6, pp. 4600–4612, 2019.
[28] A. Levant, "Higher-order sliding modes, differentiation and output-feedback control," *International Journal of Control*, vol. 76, no. 9-10, pp. 924–941, 2003.
[29] J. Duan, Y. Gan, M. Chen, and X. Dai, "Adaptive variable impedance control for dynamic contact force tracking in uncertain environment," *Robotics and Autonomous Systems*, vol. 102, pp. 54–65, 2018.

Linyan Han received her MSc degree in Control Theory and Control Engineering from Nanjing University of Aeronautics and Astronautics, Nanjing, China, in 2017. She is currently working towards the Ph.D in the School of Automation, Southeast University, Nanjing, China. Her interests include force control, position control, nonlinear control theory and their applications to robotic systems.

Jianliang Mao received the B.Sc., M.Sc., and Ph.D. degrees from the School of Automation, Southeast University, Nanjing, China, in 2011, 2014, and 2018, respectively. From 2018 to 2021, he worked at the Research and Development Institute, Estun Automation Co., Ltd. He was selected into "Jiangsu Province entrepreneurship and innovation plan" in 2019. He is now with the College of Automation Engineering, Shanghai University of Electric Power. His research interests include interactive control and visual servoing control of robotic manipulators.

Pengfei Cao received his B.S. in automatic control from Southeast University, Nanjing, China in 2014. He is now working toward the Ph.D. degree at Southeast University. His main research interests lie in force control, human-robot interaction and motion planning.

Yahui Gan received his B.Eng. in Automation from Shandong University P.R. China in 2007 and his Ph.D. degree in Control Theory and Control Engineering from Southeast University P.R. China in 2014. Since 2014, He has been working at the School of Automation, Southeast University and currently as an Associate Professor there. His research interest covers robot intelligent control system, human robot interaction and multiple robots cooperation.

Shihua Li (SM'10-F'20) received his B.S., M.S. and Ph.D. degrees all in Automatic Control from Southeast university, Nanjing, China in 1995, 1998 and 2001, respectively. Since 2001, he has been with School of Automation, Southeast University, where he is currently a professor and the director of Mechatronic Systems Control Laboratory. His main research interests lie in modeling, analysis and nonlinear control theory with applications to mechatronic systems, including manipulator, robot, AC motor, power electronic systems and others.